AIP | Applied Physics Letters

Design for high-power, single-lobe, grating-surface-emitting quantum cascade lasers enabled by plasmon-enhanced absorption of antisymmetric modes

C. Sigler, J. D. Kirch, T. Earles, L. J. Mawst, Z. Yu, and D. Botez

Citation: Applied Physics Letters **104**, 131108 (2014); doi: 10.1063/1.4869561
View online: http://dx.doi.org/10.1063/1.4869561
View Table of Contents: http://scitation.aip.org/content/aip/journal/apl/104/13?ver=pdfcov
Published by the AIP Publishing

APPLIED PHYSICS LETTERS 104, 131108 (2014)

Design for high-power, single-lobe, grating-surface-emitting quantum cascade lasers enabled by plasmon-enhanced absorption of antisymmetric modes

C. Sigler,[1] J. D. Kirch,[1] T. Earles,[2] L. J. Mawst,[1] Z. Yu,[1] and D. Botez[1,a)]
[1]*Department of Electrical and Computer Engineering, University of Wisconsin-Madison, 1415 Engineering Drive, Madison, Wisconsin 53706, USA*
[2]*Intraband, LLC, 200 N. Prospect Ave, Madison, Wisconsin 53726, USA*

(Received 1 January 2014; accepted 12 March 2014; published online 3 April 2014)

Resonant coupling of the transverse-magnetic polarized (guided) optical mode of a quantum-cascade laser (QCL) to the antisymmetric surface-plasmon modes of 2nd-order distributed-feedback (DFB) metal/semiconductor gratings results in strong antisymmetric-mode absorption. In turn, lasing in the symmetric mode, that is, surface emission in a single-lobe far-field beam pattern, is strongly favored over controllable ranges in grating duty cycle and tooth height. By using core-region characteristics of a published 4.6 μm-emitting QCL, grating-coupled surface-emitting (SE) QCLs are analyzed and optimized for highly efficient single-lobe operation. For infinite-length devices, it is found that when the antisymmetric mode is resonantly absorbed, the symmetric mode has negligible absorption loss ($\sim$0.1 cm^{-1}) while still being efficiently outcoupled, through the substrate, by the DFB grating. For finite-length devices, 2nd-order distributed Bragg reflector (DBR) gratings are used on both sides of the DFB grating to prevent uncontrolled reflections from cleaved facets. Equations for the threshold-current density and the differential quantum efficiency of SE DFB/DBR QCLs are derived. For 7 mm-long, 8.0 μm-wide, 4.6 μm-emitting devices, with an Ag/InP grating of $\sim$39% duty cycle, and $\sim$0.22 μm tooth height, threshold currents as low as 0.45 A are projected. Based on experimentally obtained internal efficiency values from high-performance QCLs, slope efficiencies as high as 3.4 W/A are projected; thus, offering a solution for watt-range, single-lobe CW operation from SE, mid-infrared QCLs. © *2014 AIP Publishing LLC*. [http://dx.doi.org/10.1063/1.4869561]

Grating-coupled surface-emitting lasers (GCSEL) are attractive sources due to easy packaging, lack of emitting-facet heating and subsequent degradation, ability to reach 1 W diffraction-limited continuous-wave (CW) power,[1] and the potential for obtaining multi-watt CW diffraction-limited power when combined with single-lateral-mode, high-index-contrast photonic-crystal structures.[2]

Research on GCSELs started in the early 1970s and was focused on near-infrared (IR)-emitting devices.[3–6] It was found for TE-polarized lasers that, in accordance with theory,[7] the longitudinal mode favored to lase is the antisymmetric one (i.e., a mode whose far-field pattern consists of two lobes) due to its inherent low radiation loss and subsequent low threshold gain. Several approaches have been proposed and demonstrated for realizing operation in a single-lobe beam[8] with the most successful ones being those involving no penalty in efficiency: central grating π phase shift[9–11] or chirped grating corresponding to a π phase shift.[1]

With the advent of quantum cascade lasers (QCLs) in the mid 1990s, GCSEL analysis turned to devices generating transverse-magnetic (TM)-polarized light.[12] SE distributed-feedback (DFB) grating, mid-IR-emitting QCLs include: two-dimensional (2-D) photonic-crystal structures,[13] air-metal/semiconductor gratings,[14] metal/semiconductor gratings for emission only through the substrate,[15,16] metal/semiconductor biperiodic gratings,[17] and all-semiconductor gratings.[18,19] By and large, the antisymmetric mode was found to be favored to lase, just like for TE-polarized GCSELs, with two exceptions: (a) excitation of a 2nd-order DFB region from a 1st-order DFB laser[16] which gave a single, diffraction-limited beam only for short ($\leq$200 μm) apertures and (b) an edge- and surface-emitting device[19] that provided 100 mW CW surface-emitted power in a near-diffraction-limited beam, with significant power being edge emitted, and occasional two-lobed beams due to uncontrolled facet reflections. 500 mW CW surface-emitted power was reported from ring-cavity devices,[18] but operating multimode. More recently,[20] ring-cavity GCSE QCLs have provided a symmetric-like, multilobe beam pattern, as a result of employing two π phase shifts and a linear-polarization scheme. THz SE-DFB QCLs have been found to operate in the antisymmetric mode as well with the solution for single-lobe operation being either a central π phase shift[21,22] or symmetric-mode selection via dual-slit unit-cell gratings[23] or gratings chirped from their centers to their edges.[24] Furthermore, by using resonant leaky-wave coupling,[25,26] 2-D GCSE THz QCLs emitting in diffraction-limited beams have been demonstrated.[27,28]

Here, we present a GCSE QCL mid-IR-emitting structure with inherent suppression of the antisymmetric modes that allows symmetric-mode lasing at low (<0.5 A) threshold currents and high (>3 W/A) slope efficiencies. The device relies on the antisymmetric modes being strongly absorbed due to resonant coupling of the (guided) optical mode to the antisymmetric surface plasmon mode of a metal/semiconductor grating. In addition, the DFB grating is bounded by 2nd-order

[a)]Author to whom correspondence should be addressed. Electronic mail: botez@engr.wisc.edu.

distributed Bragg reflector (DBR) gratings;[1,8–10] thus, preventing uncontrolled reflections from cleaved facets, which can affect the DFB operation,[19] as well as catastrophic facet degradation at high powers due the thermally induced sheer stress.[29] By considering a 4.6 μm-emitting QCL structure which was previously reported to edge-emit watt-range CW power,[30] we find that 7.03 mm-long DFB/DBR GCSE devices can have threshold currents as low as 0.45 A and slope efficiencies as high as 3.4 W/A; thus, making it possible to obtain watts of CW diffraction-limited, single-lobe power from mid-IR surface-emitting QCLs. First, we analyze devices of infinite-length metal/semiconductor 2nd-order DFB gratings, in order to elucidate the mechanism via which the antisymmetric mode is suppressed. Then, we present the design and analysis of 2nd-order DFB/DBR devices of finite-length gratings, and provide examples of high-performance devices.

The antisymmetric surface plasmon mode at the interface(s) of a 2nd-order metal/semiconductor has its H-field intensity nulls occur in the middle of the grating troughs and peaks [see example in Fig. 1(b)]. For an infinite-length grating with Ag for metal, InP for semiconductor and designed to be the 2nd-order DFB grating for a published[30] 4.6 μm-emitting QCL structure, we plot in Fig. 1(a) the wavevector of the plasmon as a function of grating duty cycle, defined as the percentage of metal in a grating period, and grating tooth height. A thin white line indicates the plasmon-wavevector curve corresponding to 4.6 μm wavelength, λ; that is, where the DFB-QCL structure's optical-mode propagation constant matches the plasmon-mode propagation constant, and thus resonant coupling occurs between the two modes. We show in Fig. 1(b)

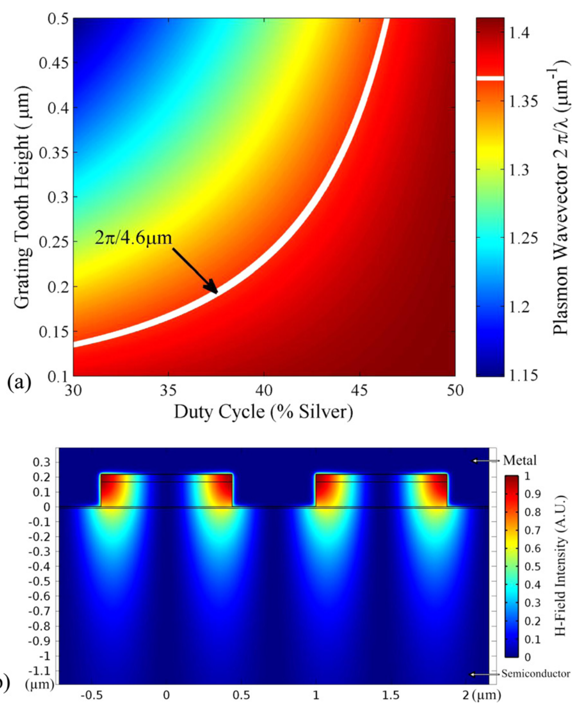

FIG. 1. Infinite-length grating: (a) Plasmon wavevector as function of grating duty cycle and tooth height for Ag/InP grating designed to be 2nd-order DFB grating for a published 4.6 μm-emitting QCL.[30] The white line corresponds to resonant coupling between the (guided) optical mode and the antisymmetric plasmon mode; (b) H-field intensity pattern at a resonance point: 39% duty cycle and 0.217 μm grating tooth height, at $\lambda = 4.6\ \mu$m.

the plasmon H-field intensity for a grating of 39% duty cycle and 0.217 μm tooth height ($\lambda = 4.6\ \mu$m).

Next, we consider the DFB-QCL structure for which the (transverse) optical mode couples to the grating surface-plasmon modes. Coupling to the antisymmetric and symmetric plasmon modes results in antisymmetric (A) and symmetric (S) longitudinal modes of the structure. We choose a 40-period, 4.6 μm-emitting QCL structure[30] of 75% transverse optical-confinement factor Γ. The grating period Λ is fixed to be that ratio of the vacuum wavelength (4.6 μm) to the effective refractive index of the transverse mode, such that the 2nd-order Bragg-diffraction condition is met. For this 2nd-order DFB-QCL structure, we show in Fig. 2 the dispersion curves, at 39% grating duty cycle, for the A and S modes as a function of tooth height, h. As seen from the inserted pictures, in the case of the A mode for $h < 0.217\ \mu$m the guided mode couples in-phase with the antisymmetric plasmon mode, while for $h > 0.217\ \mu$m the guided mode couples out-of-phase with the antisymmetric plasmon mode. The S mode couples weakly to the symmetric plasmon mode, as evidenced by negligible field at the grating interfaces. (However, the S-mode couples strongly to the grating and is effectively outcoupled over a large range in h [Fig. 3(b)].) Such modal behavior is somewhat similar to that for the modes of 1st-order metal/semiconductor DFB structures,[31] in that the A and S modes qualitatively behave like the 1st-order DFB modes whose H-field maxima occur on the grating troughs and peaks, respectively (Fig. 3 in Ref. 31).

Fig. 3(a) shows the A-mode loss as a function of grating height and duty cycle. We superimpose the white line from Fig. 1(a) on the locus of maximum-loss points, to highlight that the latter corresponds to resonant coupling between guided and plasmon modes. The losses for the A and S modes are shown in Fig. 3(b) as the grating height varies, when the duty cycle is 39%. The A-mode loss is only absorption loss which is peaked at resonance (i.e., at $h = 0.217\ \mu$m). The S mode has both surface-emission (coupling coefficient $\kappa = 0.193 - i9.231\ \mathrm{cm}^{-1}$) and absorption losses; the latter being negligible ($\sim 0.1\ \mathrm{cm}^{-1}$) due to weak optical-mode coupling to the symmetric plasmon mode. We note that significantly enhanced absorption of incident TM-polarized light, due to strong coupling to a surface-plasmon mode of a

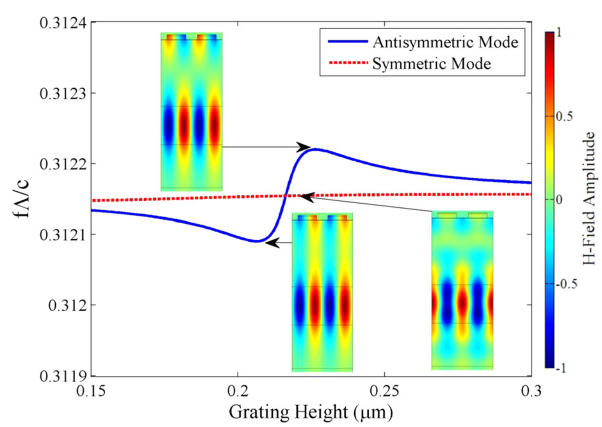

FIG. 2. Normalized frequencies for the symmetric (S) and antisymmetric (A) modes of 4.6 μm-emitting 2nd-order DFB-QCL structure, at 39% grating duty cycle, as a function of grating tooth height, h. Insets: H-field amplitude patterns. The A-mode is shown below and above resonance at $h = 0.217\ \mu$m.

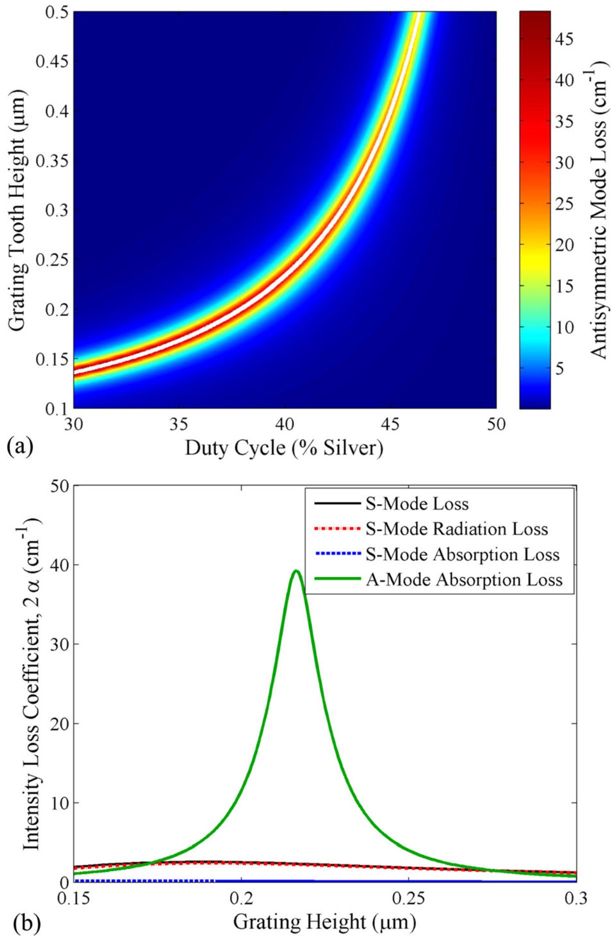

FIG. 3. (a) The antisymmetric (A)-mode loss as a function of grating duty cycle and tooth height. The white line atop the locus of maximum-loss points is the same white line as in Fig. 1(a), confirming that the A-mode maximum loss occurs at grating parameters corresponding to resonant coupling between guided and plasmon modes. (b) Intensity loss coefficient[8] for the symmetric and antisymmetric modes as a function of grating height when the grating duty cycle is 39%. The S-mode absorption loss is negligible.

2nd-order DFB metal grating, has previously been obtained[32] for proposed high-performance mid-IR photodetectors.

Next, we study finite-length, buried-heterostructure devices with DBR gratings at the ends of the DFB grating (Fig. 4), just as for high-power, near-IR GCSELs.[1,8–10] A longitudinal cross-section is shown in the inset. The 40-period InGaAs/InAlAs core region of a high-CW-power, 4.6 μm-emitting QCL[30] is considered. Atop an InP cladding layer a metal/semiconductor grating is placed. To control the tooth height, a 10 nm-thick InGaAs etch-stop layer [Fig. 1(b)] is introduced between the InP cladding layer and the grating. At the top of the semiconductor portions of the grating, a 50 nm-thick n^+-InP layer is added [Fig. 1(b)] to ensure good electrical contact, and 2 nm-thick Ti layers are inserted between metal and semiconductor for good adhesion.

For finite-length devices, the coupled-mode theory for 2nd-order metal/semiconductor gratings is employed[7] together with the matrix method for DFB/DBR structures[8] adjusted for TM-polarized light. More specifically, COMSOL is used to calculate the eigenfrequencies of the symmetric and antisymmetric modes for an infinite-length DFB structure.[7] The real and imaginary parts of these are converted into detuning and loss parameters, both in units of

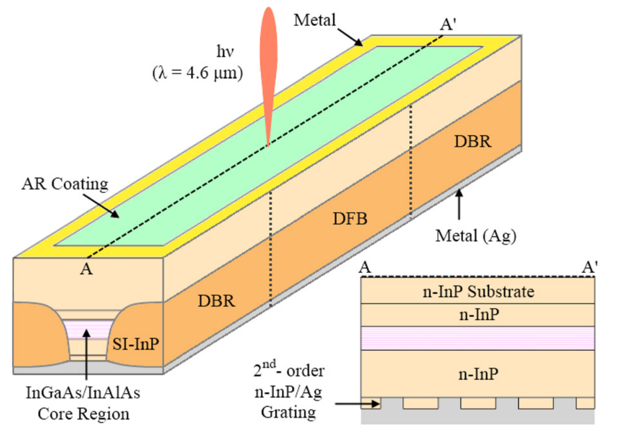

FIG. 4. Schematic representation of surface-emitting, buried-heterostructure DFB/DBR QCL for operation at 4.6 μm wavelength.

cm^{-1}, and then inserted into the equations for calculating the coupling coefficient and correction factor.[7] Then, we use the transfer-matrix method to solve for the grating-related (intensity) loss coefficient,[8] 2α, which is part of the *local* threshold gain (i.e., in the DFB region) g_{th},[2,8] which, for interband-transition devices, is given by

$$g_{th} = 2\alpha + \frac{\alpha_i}{\Gamma_{lg}}, \tag{1}$$

where α_i is the internal cavity loss and Γ_{lg} is the percentage of field intensity residing in the DFB region. However, for QCLs one has to take into account the backfilling-current density[33] and the leakage-current density[33] which, multiplied by Γg, are routinely subsumed with α_i as being parts of a "waveguide" loss coefficient α_w in the threshold-current density formula for Fabry-Perot-cavity devices: $J_{th} = (\alpha_m + \alpha_w)/\Gamma g$, where α_m is the mirror loss and g is the differential gain. Since backfilling and carrier leakage occur only in the DFB region, the g_{th} equation for SE DFB/DBR QCLs is

$$g_{th,q} = 2\alpha + \alpha_w + \left(\frac{1}{\Gamma_{lg}} - 1\right)\alpha_i. \tag{2}$$

For α_w we take the experimental value obtained[30] by Lyakh *et al.*: 3.3 cm^{-1}, and for α_i we take a value of 0.5 cm^{-1}, typical of state-of-the-art, high-power 4.5–5.0 μm-emitting QCLs.[34,35] The modal threshold gain[2] $G_{th,q} = \Gamma_{lg} g_{th,q}$. Then, the threshold-current density is

$$J_{th} = \frac{G_{th,q}}{\Gamma_{lg}\Gamma g} = \frac{g_{th,q}}{\Gamma g}. \tag{3}$$

The finite-length structure chosen for analysis is one that maximizes the outcoupling loss for the S mode, while maintaining a low value (i.e., 2) for the S-mode guided-field-intensity peak-to-valley ratio in the DFB region[8] R_0; chosen to prevent multimoding at high-drive levels due to longitudinal gain spatial hole burning. Then, for a 7.03 mm-long device of 3.07 mm-long DFB region and 1.98 mm-long DBR regions, we find for the S mode that $2\alpha = 5.98\ cm^{-1}$ and $\Gamma_{lg} = 0.81$. In turn, $g_{th,q}$ has a value of 9.4 cm^{-1} and the G_{th} value is 7.6 cm^{-1}. Fig. 5(a) shows the $g_{th,q}$ values for A and S modes, as a function of detuning from the reference 4.6 μm wavelength, for a grating of 39% duty cycle and 0.217 μm height.

An S mode is clearly favored to lase over two adjacent A modes, which have $g_{th,q}$ values $23.1\,cm^{-1}$ and $23.9\,cm^{-1}$ higher than the S mode. These large intermodal-discrimination values are dominated by the strong absorption of the A modes. For the S mode, by using Eq. (3) and the g value experimentally obtained by Lyakh *et al.*,[30] we obtain a J_{th} value of $1.84\,kA/cm^2$. Then, for a 3.07 mm-long DFB region and a 8.0 μm-wide buried-ridge guide,[36] as needed for operation primarily in the fundamental lateral mode,[37] the threshold current is 0.45 A, a value comparable to those of state-of-the-art, high-power edge-emitting QCLs operating in the 4.5–5.0 μm range.[34,35]

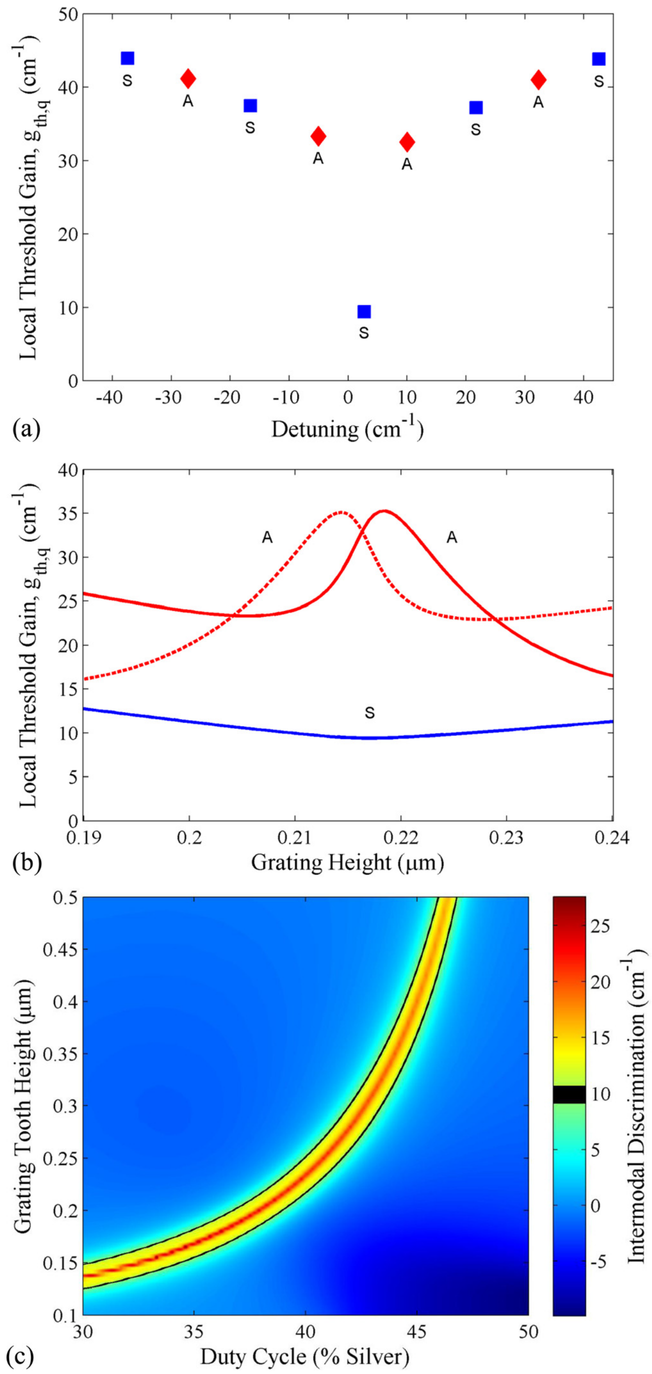

FIG. 5. (a) Local threshold gain $g_{th,q}$ for S and A modes, at 39% duty cycle and 0.217 μm grating height, as a function of detuning from the 4.6 μm reference wavelength. (b) $g_{th,q}$ for S and A modes vs. grating height, at 39% duty cycle. (c) Intermodal discrimination vs. grating height and duty cycle.

Fig. 5(b) shows the $g_{th,q}$ values for the S and the two adjacent A modes as a function of grating height, at 39% duty cycle. The A modes reach $g_{th,q}$ maxima at values corresponding to resonant coupling of the guided mode to the antisymmetric plasmon mode, at their respective oscillation wavelength. The intermodal discrimination is $\geq 10\,cm^{-1}$ over a 0.030 μm-wide variation in tooth height, which is quite achievable by using a stop-etch layer. Fig. 5(c) shows the intermodal discrimination as a function of duty cycle and tooth height. Thin black lines indicate where the intermodal discrimination is $10\,cm^{-1}$; thus, defining a curved-stripe-shaped domain over which the intermodal discrimination is $\geq 10\,cm^{-1}$. For a fixed duty cycle, intermodal discrimination is $\geq 10\,cm^{-1}$ over a 0.030 μm-wide variation in tooth height (e.g., over the 0.202–0.232 μm range in tooth height at 39% duty cycle). This can easily be achieved by using the InGaAs stop-etch layer. For a fixed tooth height, intermodal discrimination is $\geq 10\,cm^{-1}$ over a 2%-wide variation in duty cycle (e.g., over the 38%–40% range in duty cycle at 0.217 μm tooth height). For a grating of 1.44 μm period, this corresponds to controlling the tooth width within 0.03 μm, which can be achieved with e-beam lithography.

A study over the ranges: 37%–41% in duty cycle and 0.202–0.232 μm in grating height, *within* the $\geq 10\,cm^{-1}$ domain, reveals that the grating outcoupling efficiency decreases by at most 15% (i.e., from 40% to 34%). 40% outcoupling efficiency is obtained for 38%, 39% and 40% duty cycle at 0.202 μm, 0.217 μm and 0.232 μm grating height, respectively. Thus, the chance of getting outcoupling efficiencies close to 40% is high. Finally, if the grating height is controlled, via the etch-stop layer, to be within the 0.03 μm range, the range of acceptable duty-cycle values is 4%: from 37% to 41%; thus, the actual tolerance in grating-tooth width is 0.06 μm, which can be controlled via e-beam lithography.

Figs. 6(a) and 6(b) show the *radiated* near-field intensity[8,9] and the envelope of the guided-field intensity profiles for S and A modes, when the grating duty cycle and tooth height are 39% and 0.217 μm. The R_0 value is only 2, as required to ensure single-longitudinal-mode operation to high drive levels.[1,8] For the A modes the guided-field intensity in

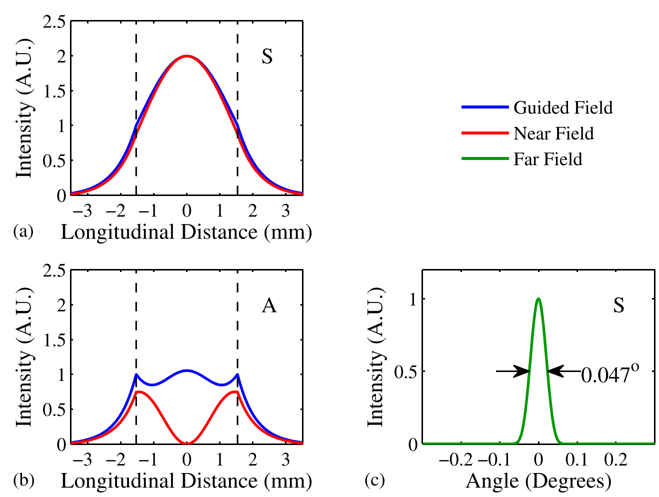

FIG. 6. Near-field intensity and envelope of guided-field intensity profiles for (a) S and (b) A modes, at 39% duty cycle and 0.217 μm grating height. (c) Far-field beam pattern for the S mode.

the DFB region is fairly uniform, yet peaks in the center of the DFB region. Considering this, the fact that the intermodal discrimination is $>20\,\text{cm}^{-1}$ and that $R_0 = 2$, it is quite reasonable to assume that longitudinal spatial hole burning is unlikely to cause multimoding at high drives above threshold. Fig. 6(c) is the S-mode far-field beam pattern: a single lobe.

As for the differential quantum efficiency, the equation for GCSELs[2,8] modified for QCLs is

$$\eta_d = \eta_i \frac{\alpha_{surf}}{G_{th}} N_p = \eta_p \eta_{tr} \frac{\alpha_{surf}}{2\alpha\Gamma_{lg} + \alpha_i} N_p, \tag{4}$$

where α_{surf} is the surface radiation loss;[2] η_{i} is the internal differential efficiency per period,[38] the product of η_{p}, the differential pumping efficiency, and η_{tr}, the transition differential efficiency; and N_{p} is the period number. The $\alpha_{\text{surf}}/\text{G}_{\text{th}}$ term, known as outcoupling efficiency, is 40% in this case. While for devices with suppressed carrier leakage (i.e., η_{p} close to unity) the η_{i} value is theoretically $\sim$0.85, the best reported[35,39] experimental values are in the 0.70–0.79 range. Then, taking $N_{\text{p}} = 40$, $\lambda = 4.6\,\mu$m, and assuming an AR-coated window and negligible substrate absorption, the estimated slope efficiencies are 3.0–3.4 W/A, values comparable to best reported pulsed, single-facet values from 4.6 μm-emitting devices. Furthermore, for devices with $R_0 = 2.5$ the outcoupling efficiency increases to 48%; then, the slope efficiencies are in the 3.6–4.1 W/A range. Since gain spatial hole burning is not well understood in QCLs, we chose to analyze the more conservative case of $R_0 = 2$, but that does not mean that devices of $R_0 = 2.5$ are not possible candidates for single-mode operation to watt-range powers.

Using the estimated threshold and slope-efficiency values (i.e., 0.45 A and 3.4 W/A), the projected peak pulsed power at 3$\times$ threshold is 3.06 W. The coherent power can be increased via resonant leaky-wave coupling of GCSE devices in the lateral direction.[2,27,28] In fact, we have recently demonstrated[40] in-phase mode lasing of five resonant leaky-wave-coupled QCLs. Then, considering that typically $\sim$67% of the coherent power is emitted in the array main far-field lobe, for a five-element phase-locked array of DFB/DBR QCLs coherent powers in excess of 10 W become possible.

In conclusion, a type of grating-surface-emitting laser is presented that offers efficient single-lobe lasing due to the antisymmetric modes being strongly absorbed via TM-mode resonant coupling to surface plasmon modes. By employing a published QCL-core structure, we find that DFB/DBR devices can lase in a single-lobe pattern with threshold currents as low as 0.45 A and slope efficiencies as high as 3.4 W/A. Thus, the devices hold potential for watt-range CW coherent-power emission delivered reliably, since emitting-facet heating and subsequent degradation are avoided.

This work was supported under Navy Contract No. N68335-11-C-0432 (K. K. Law).

[1]S. H. Macomber, J. S. Mott, B. D. Schwartz, R. S. Setzko, J. J. Power, P. A. Lee, D. P. Kwo, R. M. Dixon, and J. E. Logue, Proc. SPIE **3001**, 42 (1997).
[2]S. Li and D. Botez, IEEE J. Quantum Electron. **43**, 655 (2007).
[3]R. F. Kazarinov and R. A. Suris, Sov. Phys. Semicond. **6**, 1184 (1973).
[4]P. Zory, Appl. Phys. Lett. **22**, 125 (1973).
[5]G. A. Evans, J. M. Hammer, N. W. Carlson, F. R. Elia, E. A. James, and J. B. Kirk, Appl. Phys. Lett. **49**, 314 (1986).
[6]K. Mitsunaga, M. Kaneya, K. Kojima, S. Noda, K. Kyuma, K. Hamanaka, and T. Nakayama, Appl. Phys. Lett. **50**, 1788 (1987).
[7]R. J. Noll and S. H. Macomber, IEEE J. Quantum Electron. **26**, 456 (1990).
[8]S. Li, G. Witjaksono, S. Macomber, and D. Botez, IEEE J. Sel. Top. Quantum Electron. **9**, 1153 (2003).
[9]G. Witjaksono and D. Botez, Appl. Phys. Lett. **78**, 4088 (2001).
[10]G. Witjaksono, S. Li, J. J. Lee, D. Botez, and W. K. Chan, Appl. Phys. Lett. **83**, 5365 (2003).
[11]E. Miyai and S. Noda, Appl. Phys. Lett. **86**, 111113 (2005).
[12]N. Finger, W. Schrenk, and E. Gornik, IEEE J. Quantum Electron. **36**, 780 (2000).
[13]R. Colombelli, K. Srinivasan, M. Troccoli, O. Painter, C. F. Gmachl, D. M. Tennant, A. M. Sergent, D. L. Sivco, A. Y. Cho, and F. Capasso, Science **302**, 1374 (2003).
[14]C. Pflügl, M. Austerer, W. Schrenk, S. Golka, G. Strasser, R. P. Green, L. R. Wilson, J. W. Cockburn, A. B. Krysa, and J. S. Roberts, Appl. Phys. Lett. **86**, 211102 (2005).
[15]A. Lyakh, P. Zory, M. D'Souza, D. Botez, and D. Bour, Appl. Phys. Lett. **91**, 181116 (2007).
[16]G. Maisons, M. Carras, M. Garcia, B. Simozrag, and X. Marcadet, Appl. Phys. Lett. **98**, 021101 (2011).
[17]G. Maisons, M. Carras, M. Garcia, O. Parillaud, B. Simozrag, X. Marcadet, and A. De Rossi, Appl. Phys. Lett. **94**, 151104 (2009).
[18]Y. Bai, S. Tsao, N. Bandyopadhyay, S. Slivken, Q. Y. Lu, D. Caffey, M. Pushkarsky, T. Day, and M. Razeghi, Appl. Phys. Lett. **99**, 261104 (2011).
[19]D.-Y. Yao, J.-C. Zhang, F.-Q. Liu, N. Zhuo, F.-L. Yan, L.-J. Wang, J.-Q. Liu, and Z.-G. Wang, Appl. Phys. Lett. **103**, 041121 (2013).
[20]C. Schwarzer, R. Szedlak, S. I. Ahn, T. Zederbauer, H. Detz, A. Andrews, W. Schrenk, and G. Strasser, Appl. Phys. Lett. **103**, 081101 (2013).
[21]S. Kumar, B. S. Williams, Q. Qin, A. W. M. Lee, and Q. Hu, Opt. Express **15**, 113 (2007).
[22]G. Sevin, D. Fowler, G. Xu, F. H. Julien, R. Colombelli, S. P. Khanna, E. H. Linfield, and A. G. Davies, Appl. Phys. Lett. **97**, 131101 (2010).
[23]L. Mahler, A. Tredicucci, F. Beltram, C. Walther, J. Faist, H. E. Beere, and D. A. Ritchie, Appl. Phys. Lett. **96**, 191109 (2010).
[24]G. Xu, R. Colombelli, S. P. Khanna, A. Belarouci, X. Letartre, L. Li, E. H. Linfield, A. G. Davies, H. E. Beere, and D. A. Ritchie, Nat. Commun. **3**, 952 (2012).
[25]D. Botez, L. J. Mawst, and G. Peterson, Electron. Lett. **24**, 1328 (1988).
[26]D. Botez, L. J. Mawst, G. Peterson, and T. J. Roth, Appl. Phys. Lett. **54**, 2183 (1989).
[27]T.-Y. Kao, Q. Hu, and J. L. Reno, Appl. Phys. Lett. **96**, 101106 (2010).
[28]Y. Halioua, G. Xu, S. Moumdji, R. Colombelli, S. P. Khanna, L. Li, A. G. Davies, E. H. Linfield, H. Beere, and D. A. Ritchie, in Proceedings of 12th International Conference on Intersubband Transitions in Quantum Wells, Bolton Landing, NY, September 2013.
[29]Q. Zhang, F.-Q. Liu, W. Zhang, Q. Lu, L. Wang, L. Li, and Z. Wang, Appl. Phys. Lett. **96**, 141117 (2010).
[30]A. Lyakh, C. Pflugl, L. Diehl, Q. J. Wang, F. Capasso, X. J. Wang, J. Y. Fan, T. Tanbuk-Ek, R. Maulini, A. Tsekoun, R. Go, and C. K. N. Patel, Appl. Phys. Lett. **92**, 111110 (2008).
[31]M. Carras and A. De Rossi, Phys. Rev. B **74**, 235120 (2006).
[32]Z. Yu, G. Veronis, S. Fan, and M. L. Brongersma, Appl. Phys. Lett. **89**, 151116 (2006).
[33]D. Botez, S. Kumar, J. C. Shin, L. J. Mawst, I. Vurgaftman, and J. R. Meyer, Appl. Phys. Lett. **97**, 071101 (2010).
[34]R. Maulini, A. Lyakh, A. Tsekoun, R. Go, C. Pflügl, L. Diehl, F. Capasso, and C. K. N. Patel, Appl. Phys. Lett. **95**, 151112 (2009).
[35]Y. Bai, N. Bandyopadhyay, S. Tsao, S. Slivken, and M. Razeghi, Appl. Phys. Lett. **98**, 181102 (2011).
[36]A COMSOL analysis of 8 μm-wide buried-ridge devices showed negligible changes: a 0.3% change in grating period and, at resonance, for 39% duty cycle, changes in tooth height from 0.217 μm to 0.215 μm; thus, well within the 0.03 μm tolerance in grating tooth height.
[37]Y. Bai, N. Bandyopadhyay, S. Tsao, E. Selcuk, S. Slivken, and M. Razeghi, Appl. Phys. Lett. **97**, 251104 (2010).
[38]D. Botez, J. Shin, J. Kirch, C. Chang, L. Mawst, and T. Earles, IEEE J. Sel. Top. Quantum Electron. **19**(4), 1200312 (2013).
[39]A. Wittmann, T. Gresch, E. Gini, L. Hvozdara, N. Hoyler, M. Giovannini, and J. Faist, IEEE J. Quantum Electron. **44**, 36 (2008).
[40]J. D. Kirch, C.-C. Chang, C. Boyle, L. J. Mawst, D. Lindberg, T. Earles and D. Botez, Tech. Dig. IEEE/OSA Conference on Lasers and Electro-Optics, San Jose, California, 8–13 June 2014 (to be published).